An Optical Fiber Hydrogen Sensor Using a Palladium-Coated Ball Lens

Sahar A. Chowdhury, Ricardo Correia, Daniel Francis, Simon J. Brooks, Benjamin J. S. Jones, Alexander W. J. Thompson, Jane Hodgkinson, and Ralph P. Tatam

***Abstract*—A self-referenced optical fiber refractometer using a ball lens as a sensor head has been developed and characterized. A 350-μm ball lens created at the tip of a single mode fiber has been coated with a 40-nm optically thin layer of palladium that reacts with hydrogen to form a hydride, which has a lower reflectivity than pure palladium. Optical reflectance measurements from the tip of the ball lens were performed to determine the hydrogen response. The change in reflectivity is proportional to the hydrogen concentration in the range 0% to 1% hydrogen in air with a detection limit down to 10 ppm (1σ) in air. This technique offers a simple sensor head arrangement, with a larger sampling area ($\sim$40 times) than a typical single-mode fiber core. A statistical image analysis of a palladium film, with cracks created by accelerated failure, confirms that the anticipated sensor area for a ball lens sensor head has a more predictable reflectivity than that of a bare fiber core.**

***Index Terms*—Hydrogen, instrumentation, optical fiber application, palladium, refractive index, refractometer, sensor.**

I. Introduction

THE development of a stable, intrinsically safe and reliable hydrogen sensor is essential as a safety measure in hazardous environments since hydrogen has a wide explosive limit of 4–75% volume in air [1]. A fibre optic based hydrogen sensor offers electrical isolation, eliminating many sources of ignition that may lead to an explosion. The use of low loss optical fibres allow transmission of optical signals over many kilometres, making possible remote control of a portable sensor head. Also, the sensor head can be miniaturised to micro - scale dimensions. Previous research studies have demonstrated fibre optic sensors detecting hydrogen down to parts-per-billion level (20 ppb using an interferometric setup [2]) and achieving fast response (5 s for 4% hydrogen in air [3]). Existing fibre optic hydrogen detection techniques and their demonstrated detection limits are summarised in Table I.

Manuscript received September 7, 2014; revised November 14, 2014; accepted December 9, 2014. Date of publication December 17, 2014; date of current version April 29, 2015. This work was supported by the Engineering and Physical Science Research Council, U.K., under Grants EP/H02225X/1 and GR/T18424/1. For enquiries relating to access to the research data or other materials referred to in this article, please contact Cranfield University Library and Information Services – library@cranfield.ac.uk

S. A. Chowdhury, R. Correia, D. Francis, J. Hodgkinson and R. P. Tatam are with Engineering Photonics, School of Engineering, Cranfield University, Cranfield MK43 0AL, U.K. (e-mail: s.a.chowdhury@cranfield.ac.uk; rng.correia@cranfield.ac.uk; daniel.francis@cranfield.ac.uk; j.hodgkinson@cranfield.ac.uk; r.p.tatam@cranfield.ac.uk).

S. J. Brooks, B. J. S. Jones and A. W. J. Thomson are with AWE Plc, Aldermaston RG7 4PR, U.K. (e-mail: Simon.Brooks@awe.co.uk; Ben.Jones@awe.co.uk; Alex.Thompson@awe.co.uk).

Color versions of one or more of the figures in this paper are available online at http://ieeexplore.ieee.org.

Digital Object Identifier 10.1109/JLT.2014.2384203

TABLE I
Summary of Fibre Optic Hydrogen Sensors

Physical change on absorption of H_2	Sensor details	Limit of detection	Response time	Recovery time	Ref
INTERFEROMETER BASED					
Pd expansion → strain → increase in optical path length	Mach-Zehnder interferometer Coating: 10 nm Ti/1 μm Pd	20 ppb [a]	30 s	Not stated	[2]
	50 μm Fabry-Perot cavity Coating: 2 μm Pd	35 ppm [a]	< 5 s (for 0.5%)	Not stated	[4]
INTENSITY BASED					
Pd refractive index decrease → decrease in Fresnel reflection	Surface Plasmon Resonance (SPR) Coating: 35 nm Au/180 nm SiO_2/3.75 nm Pd	0.5% [b]	< 15 s	10 s (for 4%)	[5]
	Micromirror in MMF Coating: 10 nm PdAg	< 500 ppm [a]	< 20 min	Not stated	[6]
	Micromirror on GRIN lens Coating: 10 nm Ni/150 nm PdAg / 25 nm Pt	50 ppm [c]	< 200 min	∼20 min	[6]
	Evanescent wave Coating: 10 nm PdAu	0.2% [a]	15 s (for 4%)	∼3 min(for 2%)	[7]
	Evanescent wave Coating: alternate layers of 1.4 nm Pd/0.6 nm Au	0.8% [a]	5 s (for 4%)	13 s	[3]
FIBRE GRATING BASED					
Pd expansion → strain →shift in transmission spectrum	Fibre Bragg Grating (FBG). Sensor: 300 μm Pd half-tube	10 ppm[a]	16 days (for 650 ppm)	7 days	[8], [9]
	Long Period Grating (LPG) Coating: 40 nm Pd	625 ppm [a] (75 °C)	10 s	166 s	[8]

[a] in N_2
[b] in Ar
[c] in transformer oil

Palladium is commonly used as the sensing element in a hydrogen sensor due to its high catalytic activity and high solubility of hydrogen. It reacts with hydrogen to form palladium hydride, which has a larger lattice constant than pure palladium. As the palladium film layer expands with the diffusion of hydrogen atoms into the lattice, the volume of free electrons decreases as do the real and imaginary parts of the complex refractive index, which causes the reflectivity of the palladium film to decrease. Optical fibre refractometers have been designed to make use of the change in reflected intensity from the junction between an optical fibre end, coated with a thin film of palladium, and the test medium. Butler [6] used a micromirror chemical sensor head with a 10 nm thin palladium film deposited at the end of a multi-mode fibre and detected hundreds of ppm hydrogen in nitrogen.

Palladium in its pure form exists in the α phase. With the formation of the palladium hydride, the system transitions to the β phase [10]. In the transition phase both the α and the β phase can coexist and the resulting expansion can cause additional strain in the metal hydride [11]. Hysteresis effects during hydrogenation and dehydrogenation can cause irreversible deformations that are manifested as cracks, pin-holes and peeling of the film. This can lead to reduced reflectivity due to surface delamination and thus deterioration in sensor performance. Use of a restricted sensor area, for example the core of a singlemode fibre, can lead to catastrophic failure if such flaws coincide with the active area. A larger sensor area allows greater coverage for the palladium deposition, which can reduce the probability of catastrophic failure resulting from cracks and improve the predictability of the sensor's performance.

Palladium based sensors have been tested for use with hydrogen dissolved in either air or nitrogen. Maier *et al.* [8] have remarked that the outer few nm of the film may form an oxide PdO_2, especially at elevated temperatures, which being catalytically inactive can reduce the sensor response.

Various approaches have been reported to increase the active area of Fresnel based refractometers and / or hydrogen sensors. A fibre optic bundle with multiple singlemode fibre ends has also been used for refractive index measurement [12]. Multimode fibres have been used by Butler *et al.* for hydrogen sensing [6] and by Suhadolnik *et al.* for refractometry of liquids [13], however such sensors may be subject to mode noise in the fibre. Finally, Butler has used the endface of a GRIN lens coated with Pd for hydrogen sensing [6], however this method requires careful alignment of the lens to the singlemode fibre.

In this paper, a refractometry technique is presented that uses a ball lens as a sensor head. Ball lenses are created in a fusion splicer, where the tip of a fibre is melted by an electric arc in a controlled process. The radius of the ball lens can be chosen to optimise the intensity of the Fresnel back-reflection from the outer surface of the ball lens that is coupled back into the singlemode fibre. This technique has the advantages of providing a simple sensor head (avoiding fibre and optics alignment) and a large sampling area compared to a cleaved single mode fibre. The ball lens is sputter coated with a 40 nm optically thin palladium film which serves as a micromirror and the hydrogen response is characterized for a range of hydrogen concentrations from 0 to 10,000 ppm hydrogen in air. The advantage of a large sensor area is further quantified by statistical analysis of a palladium film that was exposed to high pressure and concentration of hydrogen to accelerate failure. This paper expands on results first reported by Chowdhury *et al.* at the 23rd Optical Fibre Sensors conference, OFS23, in 2014 [14].

II. Principles of Operation

A. Optical Fibre Refractometry

The measurement principle is that changes in the refractive index of the external medium will induce a change in the Fresnel reflection at the silica/external interface [15]. That interface can be provided by a simple cleaved fibre endface or, as we show here, a ball lens. The reflectivity change is measured as a normalized change in intensity of the sensor head compared to a reference that is unaffected by the medium under test. Equation (1) equates the reference and probe measurements to the Fresnel reflectance at the fibre-air interface (reference fibre) and the ball lens-oil interface (probe fibre).

$$R \equiv \frac{(V_{\mathrm{ref}})}{(V_{\mathrm{probe}}) \times R_{\mathrm{norm}}} = \frac{\left((n_{\mathrm{core}} - n_{\mathrm{air}})/(n_{\mathrm{core}} + n_{\mathrm{air}})\right)^2}{\left((n_{\mathrm{core}} - n_{\mathrm{probe}})/(n_{\mathrm{core}} + n_{\mathrm{probe}})\right)^2} \quad (1)$$

where V_{ref} and V_{probe} are measured detector voltages for light reflected from the reference and sensor probe respectively, n_{core} and n_{air} are the refractive indices of the fibre core (1.45) and air (1.0) respectively, n_{probe} is the refractive index of the external medium (eg a calibration oil or a Pd film) and R_{norm} is a normalising factor established when the sensor probe is in air, $R_{\mathrm{norm}} = (V_{\mathrm{ref}})_{\mathrm{air}}/(V_{\mathrm{probe}})_{\mathrm{air}}$. The normalized change in reflectivity, $\Delta R/R_{\mathrm{air}}$, can then be calculated using equation (2).

$$\frac{\Delta R}{R_{\mathrm{air}}} = 1 - \frac{(V_{\mathrm{probe}})_{H_2}/(V_{\mathrm{ref}})_{\mathrm{air}}}{(V_{\mathrm{probe}})_{\mathrm{air}}/(V_{\mathrm{ref}})_{\mathrm{air}}} \cdot \frac{(V_{\mathrm{ref}})_{\mathrm{air}}}{(V_{\mathrm{probe}})_{\mathrm{air}}} \quad (2)$$

B. Gaussian Beam Expansion

Laser light emitted from a single mode fibre will expand radially in the direction of travel, *z,* with a Gaussian profile in a homogenous medium [16]. The beam starts to propagate at $z = 0$ from a minimum beam waist radius or spot radius, ω_0 where the beam intensity has fallen to $1/e^2$ (13.5%) of its peak and the wavefront is planar with an infinite radius of curvature, $R(z) = \infty$. The radius of curvature passes through a minimum at a finite *z* and increases as *z* is further increased. The beam radius increases as the beam expands and can be focused back into the single mode fibre core using a spherical lens. Thus a ball lens acting as a mirror with a radius of curvature that matches the wavefront curvature will allow beam expansion to a larger beam spot radius and then reflect this back into the core. This is demonstrated in Fig. 1.

The radius of curvature, $R(z)$ is defined by equation (3) for beam expansion in the ball lens medium.

$$R(z) = z\left[1 + \left(\frac{n_{\mathrm{ball}}\pi\omega_0^2}{\lambda z}\right)^2\right] \quad (3)$$

The ball lens is assumed to have a uniform refractive index n_{ball}, ω_0 is the beam waist radius, (5.2 μm for SMF28 fibre) at $z = 0$ and λ is the operating wavelength (1550 nm) [16].

For the optimum curvature of the ball lens, at which most of the reflected light will be coupled back into the core, the wavefront radius of curvature, $R(z)$ must be equal to the radius of the ball lens, $z/2$. This condition would ensure that the beam would be normally incident on the ball lens surface, and we would expect a Fresnel reflection from the latter that is dependent on the refractive index of the external medium. Fig. 2(a) shows the change in ball lens radius, $z/2$ and the wavefront radius with

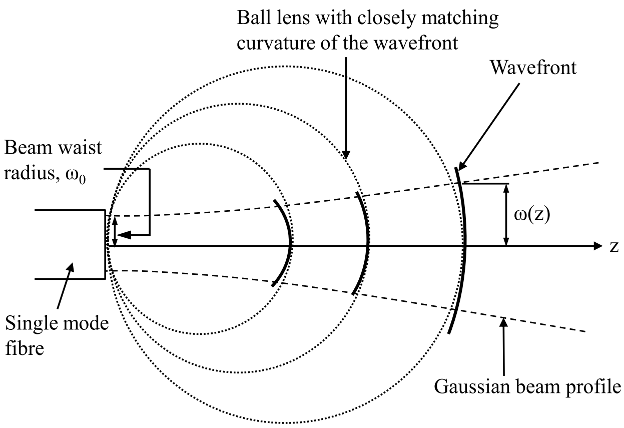

Fig. 1. Gaussian beam propagation from the output of a single-mode fibre. Construction lines representing ball lenses of various sizes are presented as well as representations of diverging wavefronts to illustrate the optimum ball lens size at which the coupling efficiency of reflected light back into the core will be maximized.

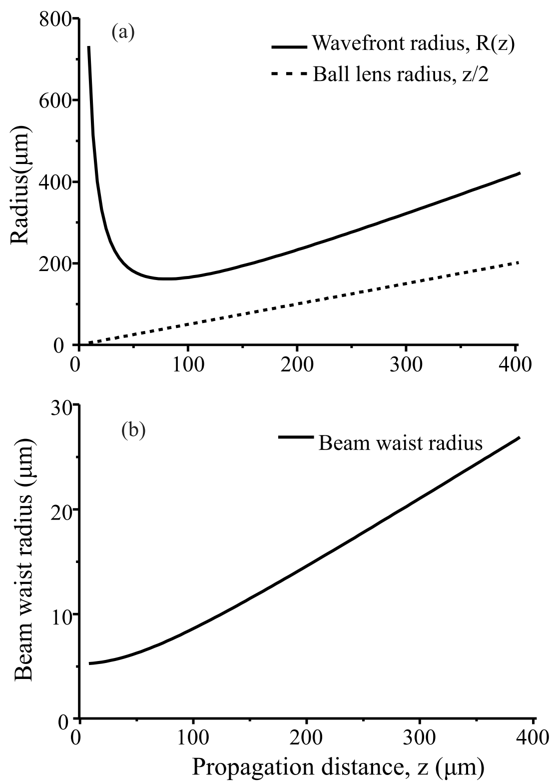

Fig. 2. (a) Change in ball lens radius, z/2 and the wavefront radius with increasing propagation distance z. (b) Beam waist radius increase with propagation distance, *z*.

increasing propagation distance *z*, calculated using equation (3). There is no point of intersection between the two traces that would allow us to maximise coupling of reflected light back into the fibre. We therefore chose to work with ball lenses at the upper end of the range supported by the fusion splicer, in order to maximise the illuminated area of the ball lens.

The evolution of the beam waist radius as a function of propagating distance, $\omega(z)$ is defined by equation (4) and displayed

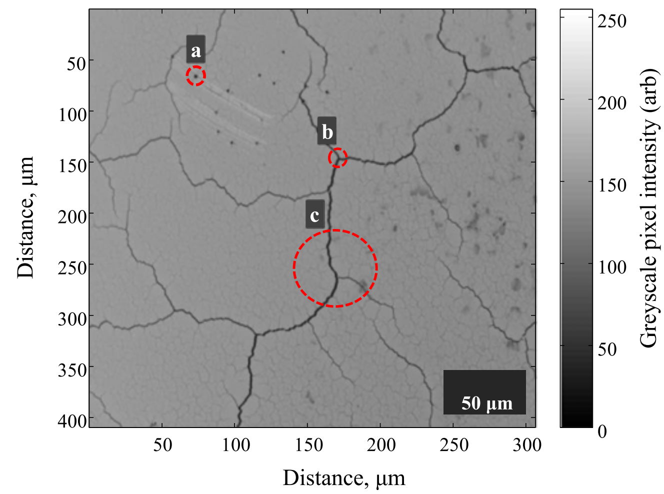

Fig. 3. Magnified image of cracked 40 nm Pd film on a glass microscope slide, taken in reflection using an optical microscope after accelerated ageing of the film (99% H_2, 100 bar, 48 hr). Circles indicate hypothetical sensors of different active area at sites a and b (both 10.4 μm diameter) and c (47 μm diameter). Circle sizes correspond to a singlemode fibre mode field diameter and ball lens spot diameter, respectively.

graphically for our system in Fig. 2(b).

$$\omega(z) = \omega_0 \left[1 + \left(\frac{\lambda z}{n_{\text{ball}} \pi \omega_0^2}\right)^2\right]^{1/2} \tag{4}$$

The beam waist radius ω_0 for wavelength is given by equations (5) and (6) [17]

$$\omega_0^2 = \frac{a^2}{\ln \nu^2} \tag{5}$$

$$\nu = \frac{2 \cdot \pi \cdot a}{\lambda_0} \sqrt{2 \cdot (n_{\text{core}} - n_{\text{clad}}) \cdot n_{\text{core}}} \tag{6}$$

where a is the radius of the SMF28 core (4.1 μm), n_{core} and n_{clad} are the refractive indices of the fibre core and cladding.

C. Quantification of Required Sensor Size

A larger area will allow a greater coverage of a palladium film layer and thus offer greater resilience to cracking of the film. To quantify this effect, a 40 nm palladium thin film deposited on a glass substrate was exposed to 99% hydrogen at 100 bar pressure for 48 hours at room temperature to accelerate failure. Fig. 3 shows an image of the cracked palladium film, taken using a microscope (Olympus, BX51) at 200 $\times$ magnification in reflection, whereby one pixel corresponds to an area of 200 nm^2. The types of cracks observed in the image are consistent with images obtained by other groups [18]. Fig. 3 shows an 8-bit greyscale image in which the low intensity pixels show irreversible pin-holes and cracks. It is possible that a singlemode fibre core could coincide with an area affected by such flaws, for example at positions *a* or *b* in Fig. 3, resulting in catastrophic failure of the sensor.

Although a larger sensor, as shown by circle *c*, is in fact more likely to have some cracks within this area, the performance of the sensor head will be more predictable because the ratio of cracked to unaffected area is more likely to be consistent. This

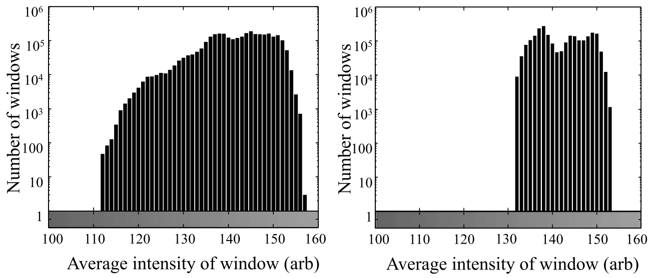

(a) (b)

Fig. 4. Histogram analysis of image in Fig. 3, following averaging over hypothetical area windows, showing relative numbers of windows with different intensity. The horizontal greyscale beneath each histogram gives a visual indication of intensity. Averaging over (a) 52×52 and (b) 240×240 pixel windows, with equivalent area to 10.4 μm and 47 μm diameter circles respectively.

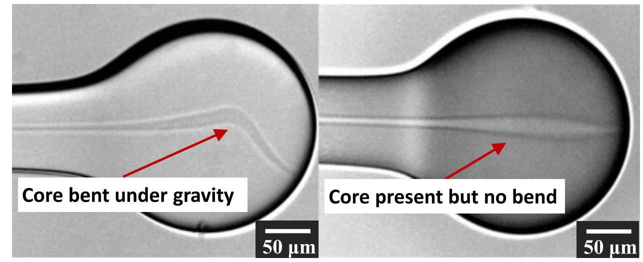

(a) (b)

Fig. 5. Effect of fibre rotation during ball lens forming; (a) tip of a single mode fibre is melted with no rotation to form a ball lens. The core is still present and its orientation affected by gravity. (b) Fibre rotated during melting creating a uniform ball lens. The core is still present but with no bending. The fibres are viewed in immersion oil that allows better contrast to see the core.

can be quantified by building an image histogram that can be treated as a discrete probability density function that defines the likelihood of a pixel intensity occurring within the image [19].

The original image was divided into a series of windows of given area (x-by-x pixels, where x is an integer). The average intensity was then calculated for each window in the entire image. The window intensities correspond to the average reflectivity that might be seen in a hypothetical sensor of the given area. The average window greyscale intensities and the number of windows with each intensity were plotted on a histogram. Fig. 4(a) shows the result of averaging over a 52×52 pixel window, which approximately corresponds to the area intersected by the single-mode fibre mode field diameter of 10.4 μm, with a mean pixel intensity of 133. Fig. 4(b) shows the result for a 240×240 pixel window, which corresponds approximately to the area intersected by the 47 μm diameter active region of a 175 μm ball lens sensor, with a mean pixel intensity of 142. As the window size increases, the number of low intensity pixels (that represent cracks) drops, resulting in a narrower histogram. Thus, larger area sensors are less likely to suffer catastrophic failure as a result of pin-holes and cracks.

III. Ball Lens Preparation

The ball lenses were made in a fusion splicer (Fujikura, FSM-100P) where the tip of the fibre was melted with an electric arc. The geometry of the ball lens is dependent on the arc power and the melting time, whereby a longer melting time led to bigger ball lenses; these parameters were controlled using the manufacturer's proprietary software [20]. The fusion splicer had an option to rotate the fibre during the melting process. An arc current of 23 mA and a melting time of ~65 s resulted in a 175 μm radius ball lens. Fig. 5(a) shows an image of a ball lens created at the tip of Corning SMF-28e fibre, which is viewed through immersion oil that matches the refractive index of the cladding. It can be observed that the core is still present and its orientation has been affected by gravity. A rotation speed of 10 °/s ensured even heat distribution during the melting process and this corrects the bending of the core, as shown in Fig 5(b). However, the reflected light can still be guided by the core, which invalidates the use of Gaussian beam expansion model in a homogeneous medium.

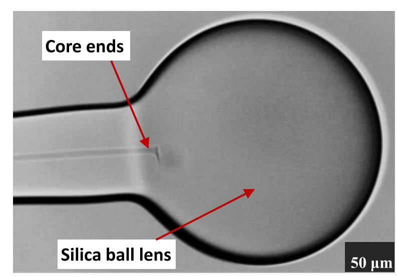

Fig. 6. Pure silica ball lens formed at the tip of a single mode fibre. SMF 28 was spliced to coreless MM125 fibre with matched 125 μm cladding diameter and the coreless fibre was melted to form the ball lens.

TABLE II
Dependence of Reflectivity on Ball Lens Radius

Measured ball lens radius (μm) ± 1 μm	Reflectivity as % of cleaved control fibre
168	ND
168.5	1.5%
174.5	10%
175.5	3%
200.5	ND
201	ND

ND: not detected; minimum detectable power 0.2%

To eliminate the presence of the core in the ball lens, a short length of coreless silica fibre (FiberCore, MM125) with a matched cladding diameter of 125 μm and a refractive index of 1.444 was spliced to the SMF-28. The MM125 fibre was melted to achieve a 175 μm radius ball lens of pure silica and uniform refractive index at the tip of the SMF-28 and is shown in Fig. 6.

We tested a range of ball lens sizes experimentally and the results are shown in Table II. Reflectivity measurements were made for different diameter ball lenses using the apparatus described later in Section IV. The optimum diameter of the ball lens is in the region of 175 ± 1 μm as can be seen from the results in Table II. Given that this does not correspond to a match between ideal ball lens radius and ideal wavefront curvature,

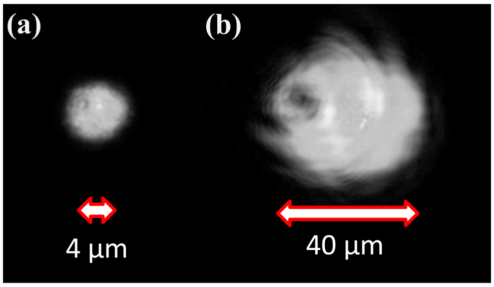

Fig. 7. Images taken from fibre ends when connected to a 532 nm laser source, using an optical microscope with 200X magnification focused onto the fibre tip. (a) Bare fibre core, SMF-28, 4 μm; (b) 175 μm radius ball lens. Calculated spot diameters at 532 nm are shown by the arrows.

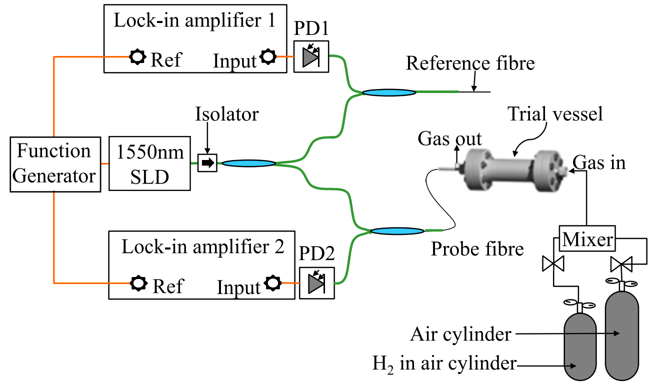

(a)

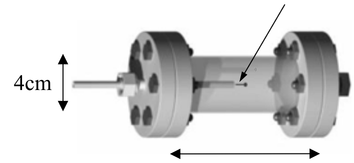

(b)

Fig. 8. (a) A referenced refractometer that uses a superluminescent diode (SLD). Light from the reference fibre and the probe fibre ending in a palladium coated ball lens is monitored by photodetector amplifiers PD1 and PD2 respectively and demodulated using lock-in amplifiers 1 and 2. (b) Transparent view of the trial vessel showing the probe fibre with ball lens.

as indicated in Fig. 2(a), these results may indicate either that there is a slight distortion in the ball lens curvature created during fabrication, or that there is some distortion of the wavefront at the end of the singlemode fibre core.

The spot sizes of the SMF-28 bare fibre and 175 μm radius ball lens were imaged under a microscope with a visible camera with 200$\times$ magnification. We employed a 532 nm green DPSS (diode pumped solid-state) laser (Photop Suwtech, model DPGL-3010 F, 10 mW output power). Fig. 7(a) and (b) show microscope images of the fibre ends. At this wavelength the calculated spot diameter of the cleaved SMF-28 is 4 μm and that of a 175 μm radius ball lens is 40 μm. We were unable to measure from the image the spot diameter where the beam intensity falls to $1/e^2$ but the calculated values are consistent with the images.

At 1550 nm, the spot diameters of the SMF-28 core and the 350 μm diameter ball lens were calculated to be 10.4 μm and 47 μm respectively, with sampling areas of 87 μm^2 and 1720 μm^2.

In an ideal case, the maximum coupling efficiency of reflected light back into the core will occur at a ball lens radius that is equal to the wavefront radius. However, as Fig. 2(a) shows, there is no ideal size of ball lens at which wavefront radius and ball lens radius intersect. Nevertheless, a ball radius of 175 μm was found to provide an acceptable level of reflectivity to permit sensor development. With the radii of curvature no longer matching, the effective sampling area of the spot size therefore becomes somewhat uncertain; we can assess the illuminated area of the sensor head, but not which parts of this area reflect light back into the core.

IV. Experimental Setup

A schematic of the Fresnel refractometer is shown in Fig. 8(a), and is similar to that reported by Dimopoulos *et al.* [15]. A 1550 nm superluminescent diode (Covega, SLD1005) was used at 500 mA with a sine-wave modulation of 9 kHz and a current amplitude of $\pm$12 mA from a function generator (Stanford Research Systems, SRS DS345). The probe fibre used a 175 μm ball lens as the sensing tip. The reference fibre used a bare cleaved fibre in air, which is insensitive to hydrogen. Fresnel reflections from the fibre ends were detected by photodetector amplifiers, PD1 and PD2 (Thorlabs, PDA10CS-EC). The photodetector signals were demodulated by matched lock-in amplifiers (Stanford Research Systems, SR850), using a time constant of 30 ms. The ratio of the probe and reference signals corrected for any time varying optical fluctuations that were common to both channels. The high modulation frequency and low time constant was used to overcome the digitization limit of the lock-in amplifiers. Although this resulted in a noisy output, the signals were later averaged over 100 data points to reduce the high frequency random noise.

Test gases were supplied from certified cylinders (BOC) with concentrations of 0 ppm (+1/-0 ppm), 998 ppm ($\pm$ 1 ppm) H_2 in air and 10,000 ppm ($\pm$100 ppm) H_2 in air. Here, "air" refers to a synthetic mixture of nitrogen and oxygen, substantially free of other trace gases. Gas from the cylinders was fed into a bank of mass flow controllers (Teledyne Hastings HFC-302 with THPS-400 controller) with ranges of (i) 0–1000 cm^3/min, (ii) 0–1000 cm^3/min, (iii) 0–100 cm^3/min and (iv) 0–10 cm^3/min. This system was used to control flow rates from the two cylinders, with downstream mixing generating a series of mixtures of different concentrations in the range 0–1000 ppm H_2 in air or 0–10,000 ppm H_2 in air. For each step change in concentration applied, a total of 6 minutes was allowed for passage of gas down the connecting pipework, diffusion into the cell and settling of the lock-in amplifiers before taking readings.

At each concentration step, signals from the probe and reference channels were recorded simultaneously and the normalised signal calculated according to equation (1). The values

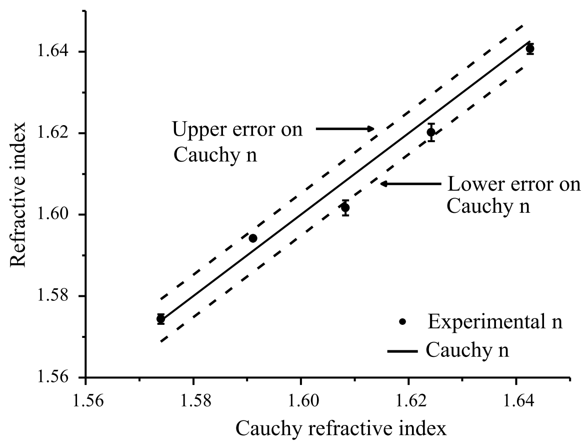

Fig. 9. Calibration chart showing the Cauchy refractive index (marked as a line with upper and lower error limits) and experimentally determined refractive index (marked as circles) with error bars.

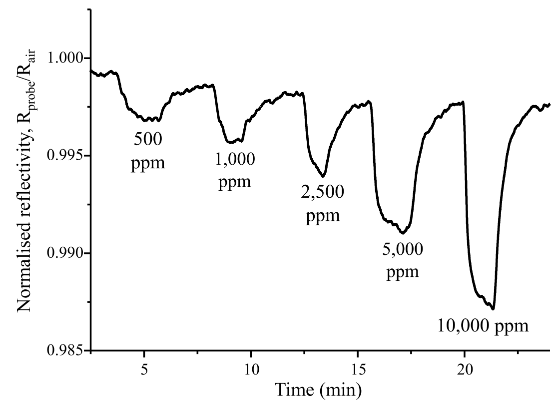

Fig. 10. Normalized reflectivity from 40nm Pd coated 175 μm ball lens exposed to various concentrations of H_2 in air. The system was flushed with air between exposures.

of $(V_{\mathrm{ref}})_{\mathrm{air}}$ and $(V_{\mathrm{probe}})_{\mathrm{air}}$ used to normalise the measurement were established in the same way by supplying zero air to the test chamber prior to each gas measurement and again taking readings simultaneously on both channels.

V. Results

A. Characterisation of the Sensor Head

To characterise the sensitivity of the ball lens as a sensor head, the uncoated ball lens was dipped in oils of known refractive index in the range 1.60 to 1.68 (Cargille Labs, Series M) measured at 589 nm and 25 °C. A Cauchy dispersion equation (provided by the manufacturer) was used to calculate the refractive index of the oils at 1550 nm and 25 °C. The resulting error in the calculated refractive index was ± 0.005 according to the manufacturer. The oils were mounted on a Peltier element to maintain a constant temperature of 25 ± 0.1 °C. The refractive index of the oils, n_{oil}, were determined from equation (1).

The oil calibration chart shown in Fig. 9 is a plot of experimentally determined refractive index using the ball lens refractometer against the calculated Cauchy refractive index values at 1550 nm and 25 °C. Each oil was experimentally measured three times and the average value plotted. The error on the data point is the standard deviation of the repeated set. The Cauchy and experimental values match closely for each oil and lie within the expected error as quoted by the manufacturer. The minimum detectable change in refractive index is 0.0012 (1σ), which is also the repeatability of the measurements and is determined by taking the average of the standard deviation of all the repeated oil measurements.

B. Hydrogen Sensing Properties

The 175 μm radius ball lens was coated with a 40 nm optically thin palladium film. A palladium film any thicker than 40 nm has been shown to have a reduced magnitude change of reflectivity [18]. The coating was fabricated using a sputter coater (Emitech K575X) with a stream of argon to provide omnidirectional deposition of sputtered atoms, in order to create films that conform to shape changes of the substrate. Our ball lenses were observed to have a Pd coating over the entire ball lens and along the exposed section of fibre (approx. 1 cm). No shadowing was visible for overhangs of less than 1 mm. However, owing to the small size of the ball lens, we were unable to confirm the coating thickness on the ball experimentally; instead, this work was performed by SEM analysis of flat microscope slides coated simultaneously.

The trial vessel used for hydrogen testing is shown in Fig. 8(b). Fig. 10 shows a typical sensor response for a range of hydrogen concentrations.

It can be observed that the voltage in air does not return to the starting baseline and this is attributed to extended recovery times. We estimated the response and recovery times as t_{90}-t_{10} where t_{10} is the time at which the signal changed by 10% of the full step, and t_{90} is the time at which the signal changed by 90% of the full step. For a change between 0 and 1000 ppm H_2, the response time was thus estimated to be 80 s and the recovery time was estimated at approximately 8 min. These times include the filling time of the test vessel and the response time of our mass flow controllers.

Extension of these measurements to other concentrations results in the data shown in Fig. 11, as the normalised change in reflectivity as a function of hydrogen concentration. The limit of detection was estimated to be 10 ppm H_2 in air (1σ). This was established as 1 standard deviation of each of two series of measurements made at 0 ppm H_2 and 10 ppm H_2. It can be seen that that the response was linear in the range 0- 10,000 ppm hydrogen in air, when the palladium hydride is in the α phase as known to happen for a thin palladium film [21].

Over the longer term, our ball lens sensor head appears to be stable, in that it has been functioning with no deterioration in performance over a period of approximately 6 months.

VI. Conclusion

A ball lens, created on the end of a single mode optical fibre and coated with a 40 nm palladium layer, has been demonstrated

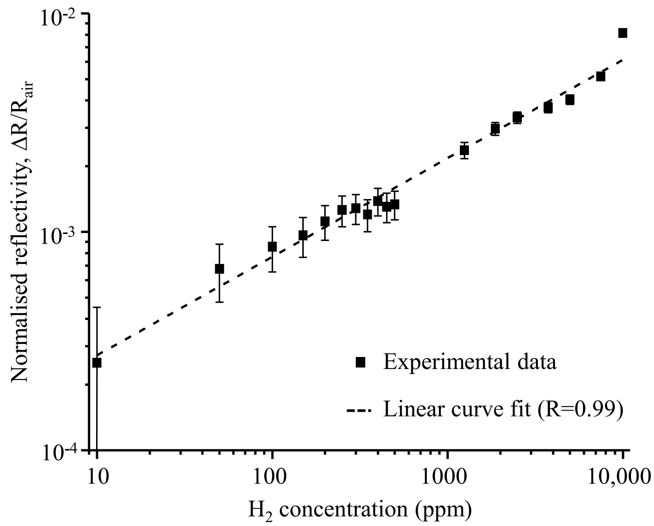

Fig. 11. Normalised change in reflectivity from the 40nm Pd coated ball lens as a function of hydrogen concentration on a log-log plot. The dotted line shows a linear fit for the data points.

as a sensor head for use in hydrogen sensing. The ball lens has an optimum radius of 175 μm at which the coupling efficiency of reflected light back into the fibre core is maximised. A refractometry technique has been applied that detects changes in reflectivity of a palladium coating as a function of hydrogen concentration from 0 to 10,000 ppm hydrogen in air. The interrogation system used a single-mode optical fibre network with two fibre channels. The probe fibre ended in a ball lens and the reference channel, which was a cleaved SMF-28 fibre, compensated for time- varying optical fluctuations that were common to both the reference and the probe channel. The detection limit was measured to be 10 ppm hydrogen in air.

Ball lenses have the advantage that they are simple to produce with no alignment issues. The large active area allows greater coverage of the palladium coating, which could offer long-term resilience to cracking and blistering compared to a bare single mode fibre core. To investigate this, we accelerated the failure of a similar Pd coating on a plain glass substrate. Statistical analysis of a microscope image of the resulting flaws has allowed quantification of this effect and shows that the larger sensing area would indeed have a more predictable reflectivity in the presence of flaws.

Acknowledgment

The authors would like to thank FiberCore UK for a sample of MM125 fibre.

References

[1] “Dealing with reported gas escapes,” Inst. Gas Eng. Managers, Derbyshire, U.K., Tech. Rep. IGE/SR/20 Edition 2, 1998.

[2] M. A. Butler and D. S. Ginley, “Hydrogen sensing with palladium-coated optical fibers,” *J. Appl. Phys.*, vol. 64, pp. 3706–3712, 1988.

[3] D. Monzón-Hernández, D. Luna-Moreno, and D. Martínez-Escobar, “Fast response fiber optic hydrogen sensor based on palladium and gold nanolayers,” *Sensor Actuators B Chem.*, vol. 136, pp. 562–566, 2009.

[4] J. S. Zeakes, K. A. Murphy, A. Elshabini-Riad, and R. O. Claus, “Modified extrinsic Fabry-Perot interferometric hydrogen gas sensor,” in *Proc. IEEE Lasers Electro-Opt. Soc. Annu. Meeting*, 1994, pp. 235–236.

[5] C. Perrotton, R. J. Westerwaal, N. Javahiraly, M. Slaman, H. Schreuders, B. Dam, and P. Meyrueis, “A reliable, sensitive and fast optical fiber hydrogen sensor based on surface plasmon resonance,” *Opt. Exp.*, vol. 21, pp. 382–390, 2013.

[6] M. A. Butler, R. Sanchez, and G. Dulleck, “Fiber optic hydrogen sensor,” Sandia Nat. Lab., Livermore, CA, USA, Tech. Rep. SAND96-113, May 1996.

[7] D. Luna-Moreno and D. Monzón-Hernández, “Effect of the Pd-Au thin film thickness uniformity on the performance of an optical fiber hydrogen sensor,” *Appl. Surf. Sci.*, vol. 253, pp. 8615–8619, 2007.

[8] R. R. J. Maier, B. J. S. Jones, J. S. Barton, S. McCulloch, T. Allsop, J. D. C. Jones, and I. Bennion, “Fibre optics in palladium-based hydrogen-sensing,” *J. Opt. A: Pure Appl. Opt.*, vol. 9, pp. S45–S59, 2007.

[9] R. R. J. Maier, J. S. Barton, J. D. C. Jones, S. McCulloch, B. J. S. Jones, and G. Burnell, “Palladium-based hydrogen sensing for monitoring of ageing materials,” *Meas. Sci. Technol.*, vol. 17, pp. 1118–1123, 2006.

[10] F. A. Lewis, “Hydrogen in palladium and palladium alloys,” *Int. J. Hydrogen Energy*, vol. 21, no. 6, pp. 461–464, 1996.

[11] T. B. Flanagan and W. A. Oates, “The effect of hysteresis on the phase diagram of Pd-H,” *J. Less-Common Met.*, vol. 92, pp. 131–142, 1983.

[12] B. Degamber and G. F. Fernando, “Process monitoring of fiber-reinforced polymer composites,” *MRS Bull.*, vol. 27, pp. 370–380, 2002.

[13] A. Suhadolnik, A. Babnik, and J. Možina, “Optical fiber reflection refractometer,” *Sens. Actuators B Chem.*, vol. 29, pp. 428–432, 1995.

[14] S. A. Chowdhury, R. Correia, D. Francis, S. J. Brooks, B. J. S. Jones, A. W. J. Thompson, J. Hodgkinson, and R. P. Tatam, “Palladium coated ball lens for optical fibre refractometry based hydrogen sensing,” *Proc. SPIE*, vol. 9157, art. no. 9157AP, 2014.

[15] A. Dimopoulos, S. J. Buggy, A. A. Skordos, S. W. James, R. P. Tatam, and I. K. Partridge, “Monitoring cure in epoxies containing carbon nanotubes with an optical-fiber Fresnel refractometer,” *J. Appl. Polym. Sci.*, vol. 113, pp. 730–735, 2009.

[16] H. Kogelnik and T. Li, “Laser beams and resonators,” *Appl. Opt.*, vol. 5, pp. 1550–1567, 1996.

[17] D. L. Lee, “Optical fibers” in *Electromagnetic Principles of Integrated Optics*. New York, NY, USA: Wiley, 1986.

[18] M. A. Butler, “Micromirror optical-fiber hydrogen sensor,” *Sensor Actuators B Chem.*, vol. 22, pp. 155–163, 1994.

[19] R. C. Gonzalez, R. E. Woods, and S. L. Eddins, *Digital Image Processing*. Knoxville, TN, USA: Gatesmark, 2009.

[20] *Fujikura Fiber Ball Lens Software, FSM-LZM-100 Ball Lens v2.0. Fujikura AFL Telecommunications, SpliceLab User’s Guide Fiber Ball-Lens Software Version 2.0*, 2013.

[21] G. A. Frazier and R. Glosser, “Characterization of thin films of the palladium-hydrogen system,” *J. Less-Common Met.*, vol. 74, pp. 89–96, 1980.

Sahar A. Chowdhury received the M.Sci. degree in physics with astronomy from the University of Nottingham, Nottingham, U.K., in 2008. She received the John Salmon M.Sci. Prize for academic excellence during the course. She then worked as an Application Developer for 3M, Bracknell, U.K., till 2011. She is currently working toward the Ph.D. degree in developing an intrinsically safe and stable fibre optic-based hydrogen sensor that can be used in explosive environments. She is a Member of the Institute of Physics and the Institute of Engineering Technology.

Ricardo Correia received the Graduate degree with a 5-year degree in instrumentation engineering from Instituto Superior de Engenharia do Porto, Portugal, in 2004 and the Ph.D. degree in the development of fibre optic sensors from Engineering Photonics, Cranfield University, Cranfield, U.K., in 2008. His doctoral research consisted of the development of a pore pressure sensor employing fibre Bragg gratings for geotechnical applications. As a Research Fellow in Engineering Photonics he has further developed FBG sensors for civil engineering and, more recently, he has developed fibre optic strain and pressure sensors for aerospace and automotive applications.

Daniel Francis is a Postdoctoral Research Fellow in Engineering Photonics, Cranfield University, Cranfield, U.K., specializing in optical instrumentation for measurement applications. His doctorate involved the development of full-field laser speckle instrumentation, for which he was awarded the Cranfield University, School of Engineering prize for best Ph.D. in 2009. His research interests include speckle interferometry, laser speckle odometry and laser spectroscopy for gas sensing. He has ten conference and journal publications and a book chapter to his name.

Simon J. Brooks received the M.Chem. degree in chemistry with Industrial Placement, from the University of Bath, Bath, U.K., in 2003 and the Ph.D. degree in supramolecular chemistry from the University of Southampton, Southampton, U.K., in 2006. He joined AWE, Reading, U.K., in 2007 to develop condition monitoring technologies and optical fibre-based sensors. He currently holds the position of Team Leader: Sensors & Spectroscopy Integration within the Materials Science Sub-Function. He is a Chartered Member of the Royal Society of Chemistry.

Benjamin J. S. Jones received the Graduate degree with a B.Sc. in marine chemistry and the Ph.D. degree in electrochemistry from the University of Wales, Bangor, in 2000 and 2004, respectively. He joined AWE, Reading, U.K., in 2004 to develop gas sensor technology and currently holds the position of Team Leader: Materials Assessment within the Materials Science Sub-Function. He is a chartered member of the Royal Society of Chemistry.

Alexander W. J. Thompson received the M.Phys. degree from the University of Oxford, Oxford, U.K., in 2009 and continued on to complete a D.Phil. degree in atomic and laser physics in 2013. He joined AWE, Reading, U.K., in 2013 as a Sensor Development Scientist within the Materials Science Sub-Function. He is a Member of the Institute of Physics and is working toward chartership.

Jane Hodgkinson received the Graduate degree with a B.A. in natural sciences from the University of Cambridge, Cambridge, U.K., in 1989 and the Ph.D. degree from the Optoelectronics Research Centre, University of Southampton, Southampton, U.K., in 1998. Following a career in the chemical, water, and gas industries, she joined Cranfield University in 2004 as a Senior Research Fellow leading the optical gas detection activity in Engineering Photonics. She is a Member of the Institute of Physics, a Chartered Physicist, Chartered Engineer, and the Chair of the UK Gas Analysis and Sensing Group.

Ralph P. Tatam received the D.Sc. degree for his research achievements in 2004 and has published more than 400 journal and conference papers. He holds a Personal Chair in Engineering Photonics in 1998 and is the Head of Engineering Photonics at Cranfield University. His research aims to develop novel optical instrumentation to better understand physical phenomena, including full field, noncontact fluid flow analysis, optical fibre sensors, sensors for autonomous vehicle odometry, embedded sensors for aerospace composite panels and optical coherence tomography. He is a Chartered Engineer, a Fellow of the Institute of Physics, a Fellow of SPIE, and has served as an elected member of the Board of Directors of SPIE (2010–2012).